Available on CMS information server

CMS NOTE 2006/127

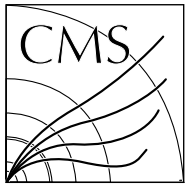

The Compact Muon Solenoid Experiment

CMS Note

Mailing address: CMS CERN, CH-1211 GENEVA 23, Switzerland

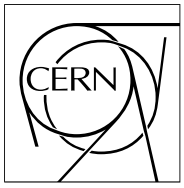

June 15, 2006

The CMS Outer Hadron Calorimeter

B. S. Acharya[1)], T. Aziz[1)], Sudeshna Banerjee[1)], Sunanda Banerjee[1)], H. S. Bawa[2)], V. Bhandari[2)], V. Bhatnagar[2)], S. B. Beri[2)], S. R. Chendvankar[1)], P. V. Deshpande[1)], S. R. Dugad[1)], S. N. Ganguli[1)], M. Guchait[1)], A. Gurtu[1)], S. D. Kalmani[1)], M. Kaur[2)], J. M. Kohli[2)], M. R. Krishnaswamy[1)], A. Kumar[2)], M. Maity[1)3)], G. Majumder[1)], K. Mazumdar[1)], N. K. Mondal[1)], P. Nagaraj[1)], V. S. Narasimham[1)], M. R. Patil[1)], L. V. Reddy[1)], B. Satyanarayana[1)], S. Sharma[1)], B. Singh[2)], J. B. Singh[2)], K. Sudhakar[1)], S. C. Tonwar[1)], P. Verma[1)]

Abstract

The CMS hadron calorimeter is a sampling calorimeter with brass absorber and plastic scintillator tiles with wavelength shifting fibres for carrying the light to the readout device. The barrel hadron calorimeter is complemented with a outer calorimeter to ensure high energy shower containment in CMS and thus working as a tail catcher. Fabrication, testing and calibrations of the outer hadron calorimeter are carried out keeping in mind its importance in the energy measurement of jets in view of linearity and resolution. It will provide a net improvement in missing $\mathrm{E_T}$ measurements at LHC energies. The outer hadron calorimeter has a very good signal to background ratio even for a minimum ionising particle and can hence be used in coincidence with the Resistive Plate Chambers of the CMS detector for the muon trigger.

[1)] Tata Institute of Fundamental Research, Mumbai

[2)] Panjab University, Chandigarh

[3)] Now at Vishwabharati University, Santiniketan

1 Introduction

The Compact Muon Solenoid (CMS) experiment [1] at the Large Hadron Collider (LHC) at CERN is designed to look for signatures of the Higgs boson, super-symmetric particles and other new physics processes in pp collisions at a centre of mass energy of 14 TeV. Signature for production of many of these new particles is large missing transverse energy, E_T measured in the detector. The momenta of all charged particles are measured using a high resolution tracker in a 4 Tesla solenoidal magnetic field, while energies of all particles, charged as well as neutral are measured using electromagnetic and hadron calorimeters. Key elements in improving the missing transverse energy measurement are hermiticity of the calorimeter, excellent energy resolution and small leakage.

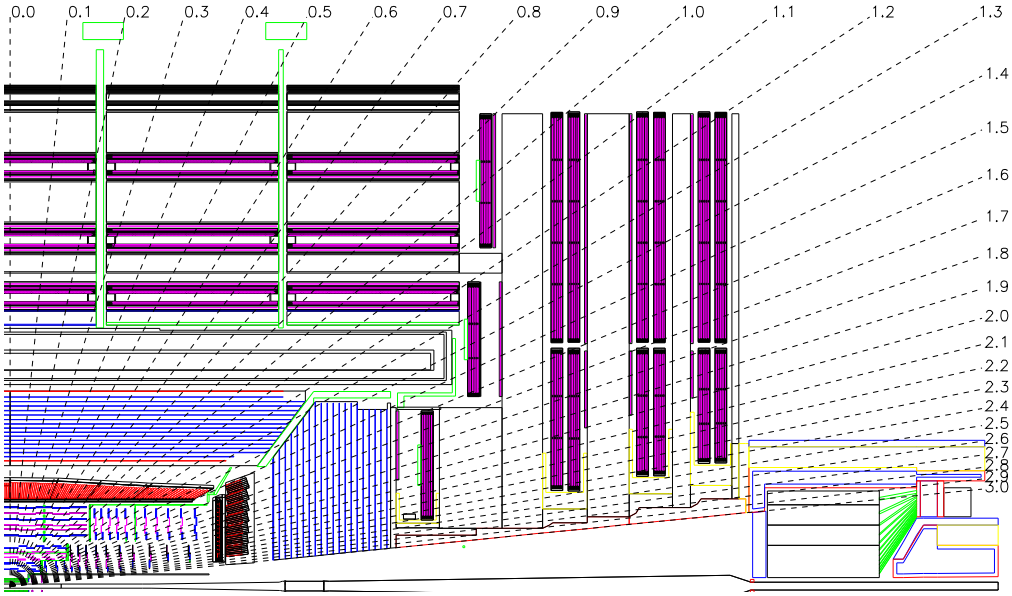

Figure 1: Longitudinal view of the CMS detector along with some fixed η lines.

Figure 1 shows the longitudinal view of the CMS detector. The dotted lines are at some fixed η values. The hadron calorimeter [2], sitting behind the tracker and the electromagnetic calorimeter as seen from the interaction point, is a sampling calorimeter made of copper alloy [1)] absorber and plastic scintillators. The barrel hadron calorimeter (HB) has a polygonal structure. It is made out of two halves, each being an assembly of 18 wedges. Each wedge subtends 20° in ϕ and is 4.33 m long along the z-direction. There are 17 slots at constant radial gaps and each of the slots houses scintillator megatiles. HB extends up to $|\eta| = 1.3-1.4$.

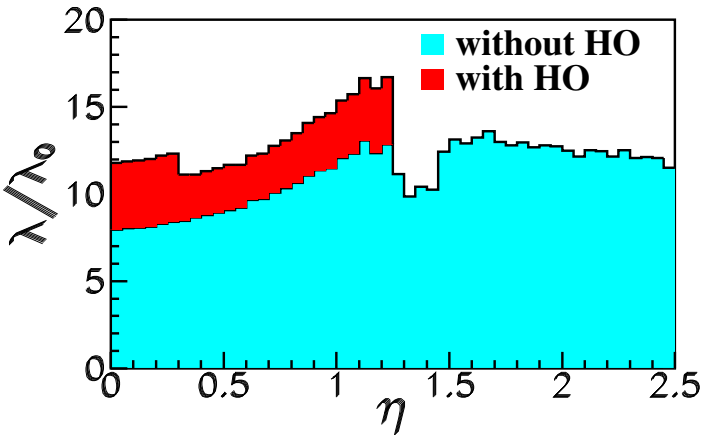

Figure 2: Number of interaction lengths till the last sampling layer of the hadron calorimeter as a function of η. The two shaded regions correspond to the setups with or without the outer hadron calorimeter (HO).

[1)] Cartridge brass # 260 with 70% Copper and 30% Zinc

HB is radially restricted between the outer extent of the electromagnetic calorimeter (R = 1.77 m) and the inner extent of the magnet coil (R = 2.95 m). This constrains the total amount of material which can be put in to absorb the hadronic shower. The amount of material till the last layer of hadron calorimeter can be seen in Figure 2 where number of interaction lengths has been plotted as a function of η. One sees the number of interaction lengths at η = 0 is close to 8 with HB alone.

An extensive study with test beam was carried out during 1995 and 1996 [3] to define the parameters of the hadron calorimeter. It was noticed (see Figure 3) that with a configuration of HB alone together with the tracker and the electromagnetic calorimeter, nearly 3% of events having a 300 GeV pion will give rise to missing energy corresponding to 100 GeV. This large fluctuation of the leakage energy can be avoided by adding layers of detectors beyond the solenoid magnet (the solenoid thickness is $1.4\lambda_{int}$). This is the primary justification for the outer hadron calorimeter.

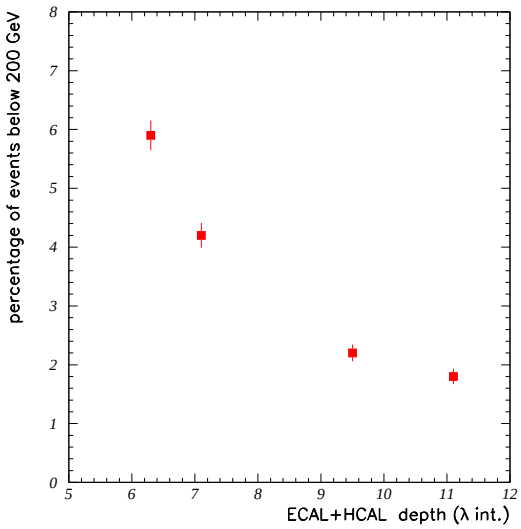

Figure 3: Fraction of 300 GeV pion data with reconstructed energy less than 200 GeV (approximately 3σ below the mean, or 100 GeV missing energy) versus total absorber depth obtained from 1996 test beam data at 3 Tesla magnetic field. The total λ_{int} includes the contribution of the electromagnetic calorimeter.

2 The Outer Hadron Calorimeter (HO): Constraints and Expectation

As mentioned in the earlier section, HB inside the 4T solenoid is relatively thin. To ensure adequate sampling depth for $\eta < 1.4$, the hadron calorimeter is extended outside the solenoid and is called HO. HO will utilise the solenoid coil as an additional absorber equal to 1.4/sinθ interaction lengths and will be used to identify the late starting showers and to measure the shower energy beyond the geometrical reach of HB.

Outside the vacuum tank of the solenoid, the magnetic field is returned through an iron yoke designed in the form of five 2.536 m wide (along z-axis) rings. HO is placed as the first sensitive layer in each of these five rings. The rings are identified by numbers -2, -1, 0, $+1$, $+2$. The numbering increases with z and the nominal central z positions of the five rings are respectively -5.342m, -2.686m, 0, $+2.686$m and $+5.342$m. Near η = 0, HB provides minimum interaction length to the hadrons produced in pp collision. Therefore, the central ring (ring 0) has two layers of HO scintillators on either side of a 19.5 mm thick piece of iron (the tail catcher iron) at radial distances of 3820 mm and 4070 mm respectively. All other rings have a single HO layer at a radial distance of 4070 mm. The total depth of the calorimeter system is thus extended to a minimum of $11.8\lambda_{int}$ (see Figure 2) except at the barrel-endcap boundary region.

The HO is constrained by the geometry and construction of the muon system. Figure 4 shows the position of HO layers in the rings of the muon stations in the overall CMS setup. The segmentation of these detectors closely follows that of the barrel muon system. Each ring has the 12 identical ϕ-sectors. The 12 sectors are separated by 75 mm thick stainless steel beams which hold successive layers of iron of the return yoke as well as the muon system. The space between successive muon rings in the η direction and also the space occupied by the stainless steel beams in the ϕ direction are not available for HO. In addition, the space occupied by the 'chimneys' in sector 3 of ring -1, and sector 4 of ring $+1$ are also not available for HO. The chimneys are used for the cryogenic

transfer lines and power cables of the magnet system. Finally, the mechanical structures needed to position the scintillator trays further constrains HO along ϕ.

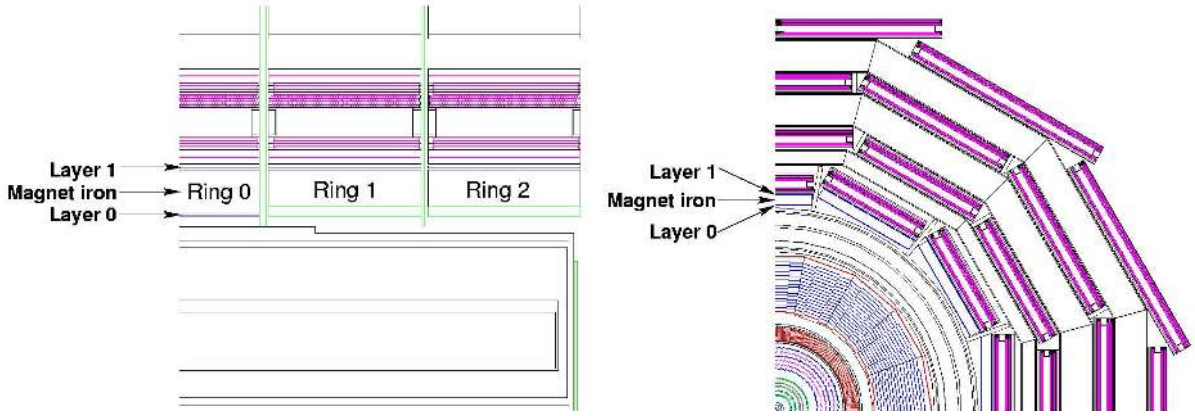

Figure 4: Longitudinal and transverse views of the CMS detector showing the position of HO layers.

In the radial direction each HO layer has been allocated a total of 40 mm space of which only 16 mm is available for the detector layer, the rest being used for the aluminium honey comb support structures on both sides of it. In addition, the HO modules are independently supported from the steel beams located on either side of each ϕ sector. The thickness and position of the iron ribs in the yoke structure further constrains the shape and segmentation of the HO.

The sizes and positions of the tiles in HO are supposed to roughly map the layers of HB to make towers of granularity 0.087×0.087 in η and ϕ. The HO consists of one (rings ± 1 and ± 2) or two (ring 0) layers of scintillator tiles located in front of the first layer of the barrel muon detector. Scintillation light from the tiles is collected using multi-clad Y11 Kuraray wave length shifting (WLS) fibres, of diameter 0.94 mm, and transported to the photo detectors located on the structure of the return yoke by splicing a multi-clad Kuraray clear fibre (also of 0.94 mm diameter) with the WLS fibre. In order to simplify installation of HO, the scintillator tiles are packed into a single unit called a tray. Each tray corresponds to one ϕ slice (5° wide in ϕ). However, along the z (η) direction, a tray covers the entire span of a muon ring. Figure 5 shows a schematic view of a HO tray where one tile is mapped to a tower of HB and the optical cable from the tray is being connected to the readout box.

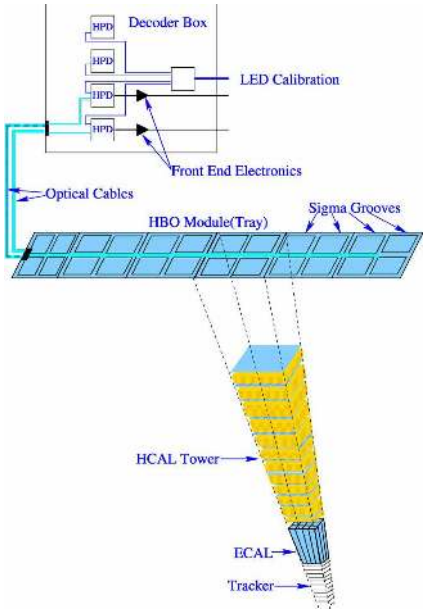

Figure 5: Schematic view of a HO tray shown with individual tiles and the corresponding grooves for WLS fibres. Each tile is mapped to a tower of HB. Optical fibres from the tray extend to the decoder box which contains the photo-detector and readout electronics.

The physics impact of HO has been studied [4] using the simulation tool CMSIM of the CMS detector. Single pions of fixed energies are shot at specific η values and the resulting energy deposits in the electromagnetic calorimeter and layers of the hadron calorimeter are combined to measure the energy. Figure 6 shows distributions of measured energy scaled to incident energy for 200 GeV pions at η = 0 and 225 GeV at η = 0.5 (pointing towards the middle of ring 1). The solid and dashed lines in the figure indicate measurements without and with HO. As can be seen in the figure, there is an excess in $\frac{\bar{E}}{E_{inc}} < 1$ for measurements without HO. This indicates the effect of leakage. The measurements with HO are more Gaussian in nature indicating that the addition of HO recovers the effect of leakage. Effect of leakage is visible at η = 0 (ring 0) from 70 GeV onwards and it increases with energy. Mean fraction of energy in HO increases from 0.38% for 10 GeV pions to 4.3% for 300 GeV pions while the RMS of the fractional energy increases from 0.034 to 0.10. There is some evidence of leakage without HO in ring 1 but with reduced intensity. The amount of leakage in ring 2 is found to be negligible.

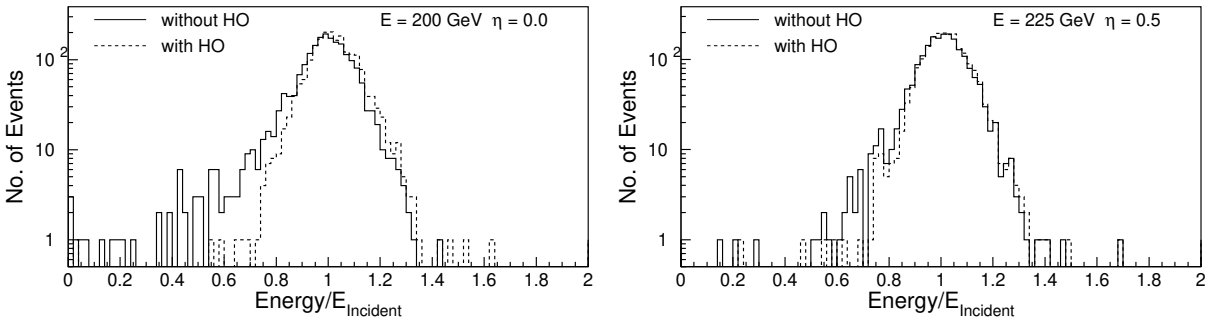

Figure 6: A simulation of the distribution of measured energy scaled to incident energy for pions with incident energies of (a) 200 GeV at η = 0 and (b) 225 GeV at η = 0.5. The solid and dashed histograms are measurements without and with HO.

The effect of shower leakage has a direct consequence on the measurement of missing transverse energy $\mathrm{E_T}$ in an event. Study of QCD events shows that the cross section for those events, where at least one particle has $\mathrm{E_T}$ above 500 GeV, runs into several pb. Clearly these events will be affected due to leakage of energy in the hadron calorimeter and the HO would be useful to decrease the leakage and improve the energy measurement. Figure 7 shows integrated cross section for missing $\mathrm{E_T}$ above a certain value. It is clear from the figure that the inclusion of HO reduces the background cross section by a factor of 1.5 or more for moderate $\mathrm{E_T}$ values. This $\mathrm{E_T}$ region is important for searches of supersymmetric particles.

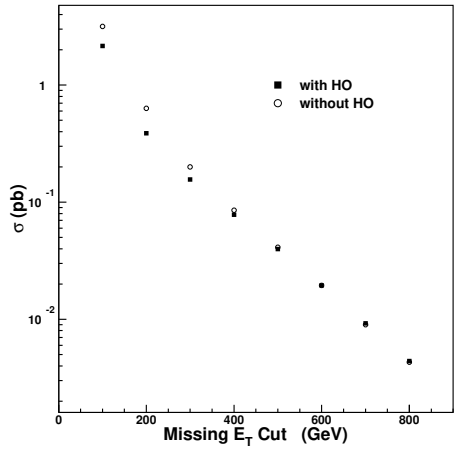

Figure 7: Integrated cross section above threshold as a function of missing $\mathrm{E_T}$ with or without HO.

3 HO Module: Design and Assembly

Panjab University and Tata Institute of Fundamental Research (TIFR) from India have undertaken the complete responsibility for the fabrication of HO. A proposal for its design and the manufacturing details was completed and reviewed in 1999 [5].

3.1 Specification

HO is physically divided into 5 rings in η conforming to the muon ring structure. The rings are numbered -2, -1, 0, $+1$ and $+2$ with increasing η. Each ring of the HO is divided into 12 identical ϕ sectors (numbered 1 to 12 counting clockwise starting from 9 O'clock position) and each sector has 6 slices (numbered 1 to 6 counting clockwise) in ϕ. The ϕ slices of a layer are identical in all sectors. The widths of the slices along ϕ are given in Table 1. In each ϕ slice, there is a further division along η. The smallest scintillator unit in HO thus obtained a called a tile. The scintillator tiles in each ϕ sector belong to a plane. Perpendicular distance of this plane from the z-axis is 3.82 m for layer 0 and 4.07 m for layer 1. The tiles in each ϕ slice of a ring are mechanically held together in the form of a tray (details in Section 3.3).

Ring	Layer	Width along ϕ in mm					
		Tray 1	Tray 2	Tray 3	Tray 4	Tray 5	Tray 6
0	0	274	343	332	327	327	268
0	1	300	364	352	347	347	292
$\pm1, \pm2$	1	317	366	354	349	349	406

Table 1: Dimension of tiles along ϕ for different trays. Each tray corresponds to one ϕ-slice in a ϕ sector.

Both layers of ring 0 have 8 η-divisions (i.e. 8 tiles in a tray): -4, -3, -2, -1, $+1$, $+2$, $+3$, $+4$. Ring 1 has 6 divisions: $5 \cdots 10$ and ring 2 has 5 divisions: $11 \cdots 15$. Ring -1 and ring -2 have the same number of divisions as rings 1 and 2 but with $-$ve indices. The η-dimensions of any tile with $-$ve tower number is the same as the one with $+$ve number. Tile dimensions along η for the towers are shown in Table 2.

Tower #	$\eta_{\max}$	Length (mm)	Tower #	$\eta_{\max}$	Length (mm)
Ring 0 Layer 0			Ring 0 Layer 1		
1	0.087	331.5	1	0.087	351.2
2	0.174	334.0	2	0.174	353.8
3	0.262	339.0	3	0.262	359.2
4	0.326	(248.8)	4	0.307	(189.1)
Ring 1 Layer 1			Ring 2 Layer 1		
5	0.436	391.5	11	0.960	420.1
6	0.524	394.2	12	1.047	545.1
7	0.611	411.0	13	1.135	583.3
8	0.698	430.9	14	1.222	626.0
9	0.785	454.0	15	1.262	(333.5
10	0.861	(426.0)			

Table 2: HO tile dimensions along η for different rings and layers. The tile sizes, which are constrained by muon ring boundaries, are mentioned in brackets.

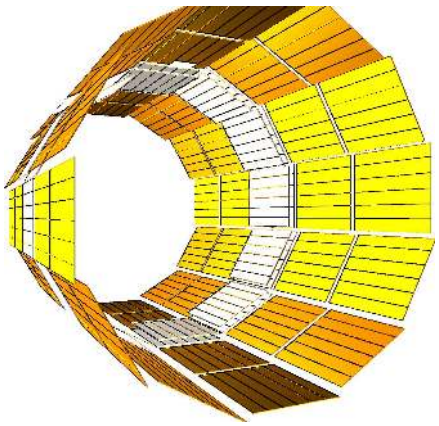

Figure 8: Layout of all the HO trays in the overall CMS detector

Figure 8 shows the final layout of all the HO trays in the overall CMS detector.Length of a full tray is 2510 mm

whereas the shorter trays, the sizes of which are constrained because of the chimney (trays 4 and 5 in sector 4 of ring $+1$ and trays 3, 4, 5 and 6 in sector 3 of ring -1), are 2119 mm long. The shorter trays are constructed without the tile corresponding to tower number ± 5. Because of the constraints imposed by the gap between the two rings, a part of tower # ± 4, which falls in ring ± 1 (tower ± 4 is restricted only to ring 0) is merged with tower # ± 5.

3.2 Tiles

Scintillator tiles are made from Bicron BC408 scintillator plates of thickness 10^{+0}_{-1} mm. Figure 9 shows a typical HO scintillator tile. The WLS fibres are held inside the tile in grooves with a key hole cross section. Each groove has a circular part (of diameter 1.35 mm) inside the scintillator and a neck of 0.86 mm width. The grooves are 2.05 mm deep. Each tile has 4 identical σ-shaped grooves, one groove in each quadrant of the tile. The grooves closely follow the quadrant boundary. The corners of the grooves are rounded to prevent damage to the fibre at the bend and to ease fibre insertion. The groove design is slightly different for the tile where the optical connector is placed at the end of the tray. Since the tiles are large, 4 grooves ensure good light collection and less attenuation of light.

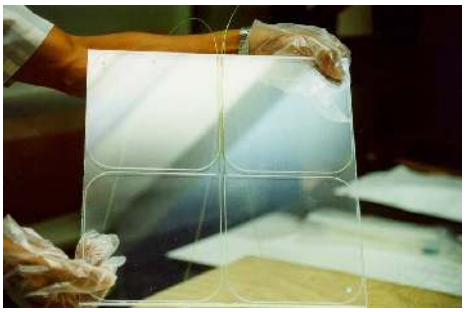

Figure 9: View of a typical tile of HO with WLS fibres inserted in the 4 σ-grooves of the tile

Machining of individual tiles is done in the following steps: (a) the plates are cut according to the size of the respective tile keeping 3 mm extra on each side; (b) the edges are trimmed to the exact dimension of the tile using a conventional milling machine; (c) grooves and screw holes are made with a CNC (Computer Numerical Control) machine; (d) σ grooves are done in two steps $-$ first a 'straight cutter' making the 0.86 mm wide 'neck' and then a 'ball cutter' making the inner circular part of the groove. The HO has 95 different tile dimensions, 75 for layer 1 and 20 for layer 0 and total number of tiles is 2730 (2154 for layer 1 and 576 for layer 0).

3.3 Trays

All tiles in each ϕ slice of a sector are grouped together in the form of a tray. Figure 10 shows a schematic view of a HO tray. Each tray contains 5 tiles in rings ± 2; 6 tiles in rings ± 1 and 8 tiles in ring 0. The edges of the tiles are painted with Bicron reflecting white paint for better light collection as well as isolating the individual tiles of a tray. Further isolation of tiles is achieved by inserting a piece of black tedlar strip in between the adjacent tiles. The tiles in a tray are covered with a single big piece of white, reflective tyvek paper. Then they are covered with black tedlar paper to prevent leakage. This package is placed between two black plastic plates for mechanical stability and ease of handling. The top plastic cover is 2 mm thick and the bottom one is 1 mm thick. Figure 11 shows a cross section of a tray to illustrate the different components. The plastic covers (top and bottom) have holes matching with the holes in the tiles. Specially designed countersunk screws passing through these holes fix the plastic covers firmly on the tiles.

The 2 mm plastic sheet on the top has 1.6 mm deep channels grooved on it (on the outer side) to route the fibres from individual tiles to an optical connector placed in a groove at the edge of the tray. A 1.5 mm wide straight groove runs along the edge of the top cover to accommodate a stainless steel tube. This is used for the passage of a radio active source for calibrating the modules. Each connector has two holes and they are fixed to the scintillator-plastic assembly through matching holes in them. Each ϕ sector in each ring has 6 trays. There are 360 trays for layer 1 and 72 trays for layer 0.

3.4 Pigtails

The light collected by the WLS fibres inserted in the tiles needs to be transported to photo detectors located far away on the muon rings. Captive ends of the WLS fibres, which reside inside the groove, are polished, aluminised

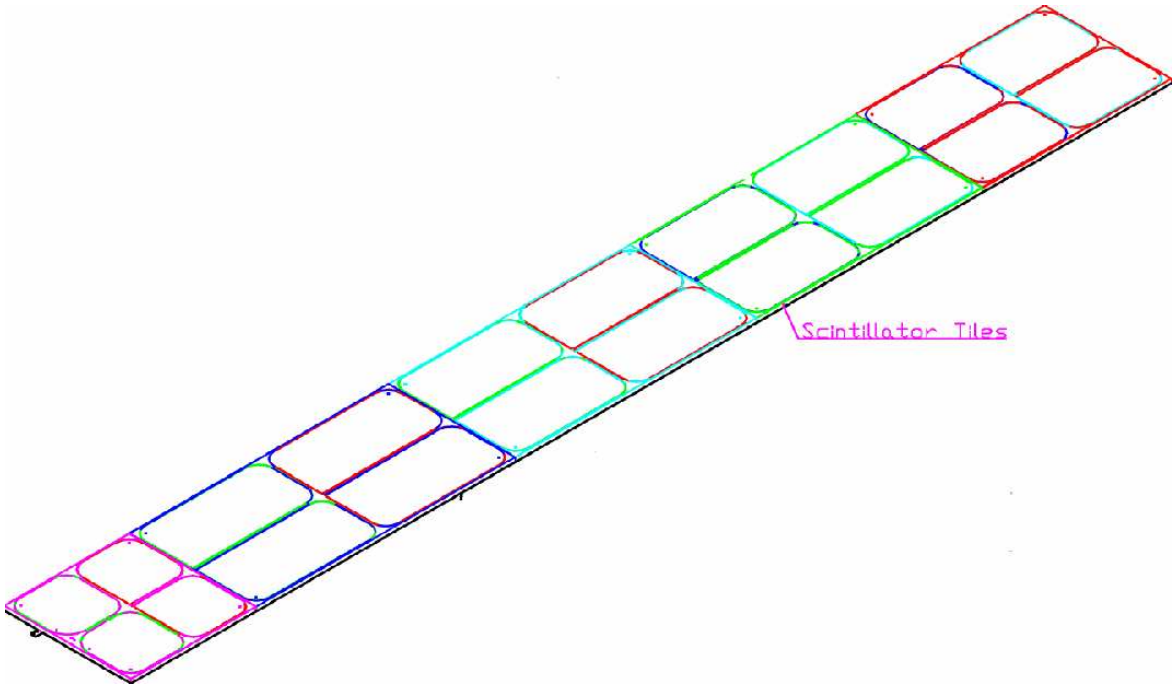

Figure 10: Layout of scintillator tiles in a typical tray of ring 2

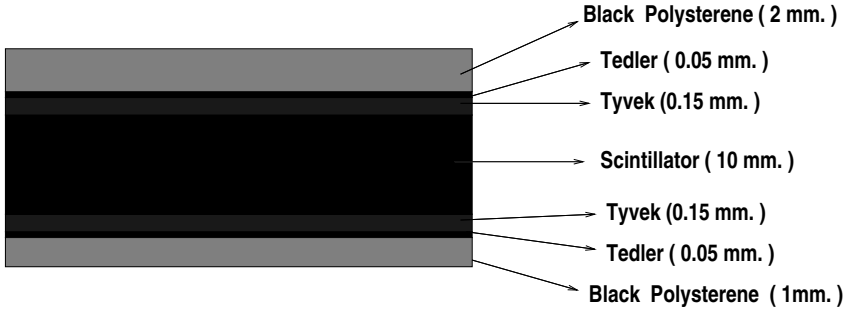

Figure 11: Cross section of a HO tray showing the different components

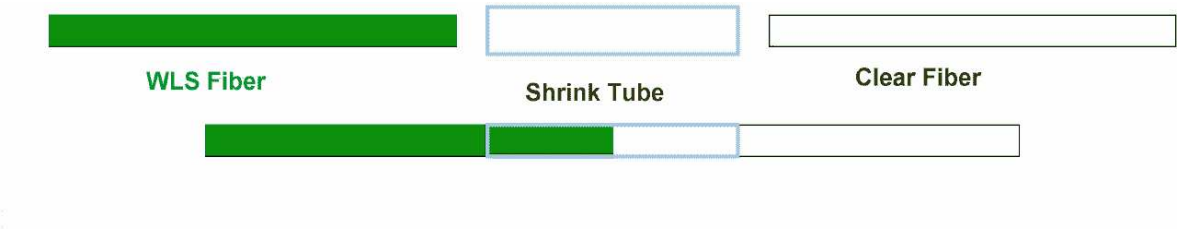

Figure 12: Illustration of splicing of a WLS fibre with a clear fibre

and protected using a thin polymer coating. The other end of the WLS fibre comes out of the tile through a slot made on the 2 mm thick black plastic cover sheet. To minimise the loss of light in transportation, the WLS fibre (attenuation length of $\sim$ 1.8 m) is spliced to a clear fibre (attenuation length of $\sim$ 8.0 m) as shown in Figure 12. A fibre is spliced only if the potential loss for using the WLS instead of a clear fibre is larger than the light loss at the spliced joint. Thus depending on tile length (along η) 2-3 fibres in each pigtail are made only of WLS fibres. The clear fibres from each tile follow the guiding grooves on the top plastic to the optical connector at the end. Each tray has two optical connectors mounted on one end of the tray. In a tray, the grooves of the tiles form two rows along η. The fibres from all grooves on one row terminate on one connector (see Figure 13). The number of fibres from trays in different rings are given in Table 3.

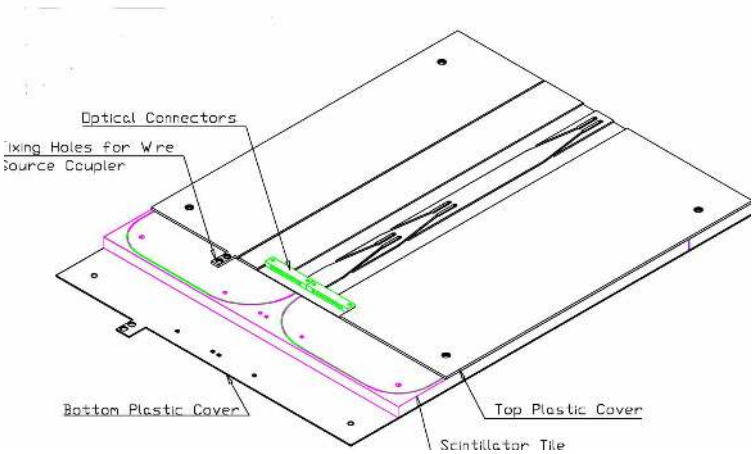

Figure 13: The arrangement of scintillation tiles, plastic covers and connectors in a tray. The components are slightly displaced from their true positions to show their matching designs

Ring #	Tiles/tray	Fibres/tray	Fibres/connector
0	8	32	16
$\pm$1	6	24	12
$\pm$2	5	20	10

Table 3: Tray specifications for different rings of HO

The bunch of fibres (WLS fibres spliced to clear fibres) fixed to the optical connector is called a pigtail (see Figure 14). Each tray has 2 pigtails and there are 864 pigtails in total: 720 for layer 1 and 144 for layer 0. Each fibre in a pigtail is cut to the proper length to match the groove length in the scintillator added to the distance from the scintillator to the optical connector at the end of the tray.

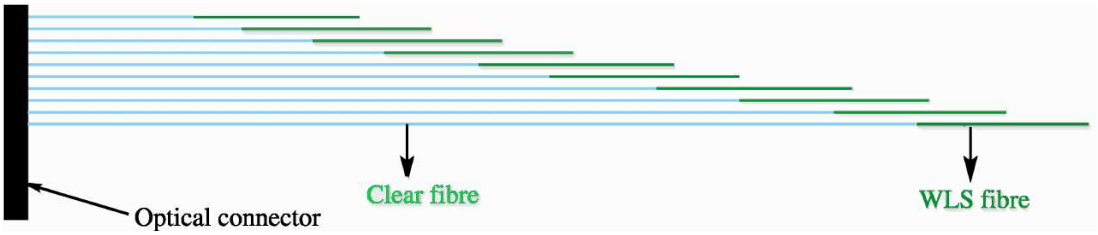

Figure 14: Illustration of an assembled pigtail (drawn not to scale)

Pigtails are made according to the following steps: (a) WLS fibres are cut according to the size of the groove in the scintillator tile; (b) both ends are polished, one end is aluminised (sputtered) and coated with a thin polymer layer; (c) clear fibre is cut with a few mm extra and one end is polished; (d) the non-sputtered end of a WLS fibre and the polished end of a clear fibre are put in a piece of heat-shrinking tube and spliced using the splicing machine; (e) spliced fibres are placed in a jig in proper order and correctly inserted in the connector with the extra length (of the clear fibres) projecting out of the connector; (f) optical cement is prepared using a resin and a hardener (Bicron BC600) and poured through the socket in the connector; (g) the pigtail is removed from the assembly jig after curing for 12 hours and the connector end is polished with a high speed diamond cutter.

3.5 Tray Assembly

The top and bottom plastic covers are sized and grooved using a CNC milling machine. Tray covers are made from 0.3 mm thick stainless steel sheets. Finally, HO trays are fabricated in the following way:

- The tiles are cleaned and their sides are painted with white (Bicron) reflecting paint for better light collection.
- Plastic covers and tray covers are also cleaned.
- Tyvek and tedlar papers are cut according to tray size and holes matching with those on the top and bottom plastic covers are punched.
- The bottom plastic sheet, tedlar and tyvek papers are placed properly and the tiles are placed on them. Two adjoint tiles are separated by strips of tedlar paper to optically isolate them. Tyvek and tedlar are folded on top, the top plastic cover is then placed and countersunk screws are used to fix the assembly of plastic covers and tiles.
- Each fibre of a pigtail is cleaned and the WLS part of the fibre is inserted carefully into the groove through the slots in top plastic cover, tedlar and tyvek. The clear fibre is routed along the groove on the top plastic cover and fixed at several places with adhesive aluminium tape.
- The optical connectors sit on their appropriate slots on the top plastic cover and are anchored with screws through holes in the plastic sheet and scintillator.
- The whole assembly is then placed inside a tray cover made out of 0.3 mm thick stainless steel sheets. This tray cover is used for transporting the trays to CERN and is removed while assembling inside the hanging structure.

4 Testing and Quality Assurance

The performance of HO depends on the quality of grooving of the tiles, painting on the sides, tray assembly, splicing and polishing of the fibres in the pigtail. All these are carefully monitored at the time of production and each completed tray undergoes a series of tests for quality assurance. Three independent quality control tests are performed: the radioactive wire-source test, radioactive XY scan, and a cosmic muon test.

4.1 Certification of Pigtails

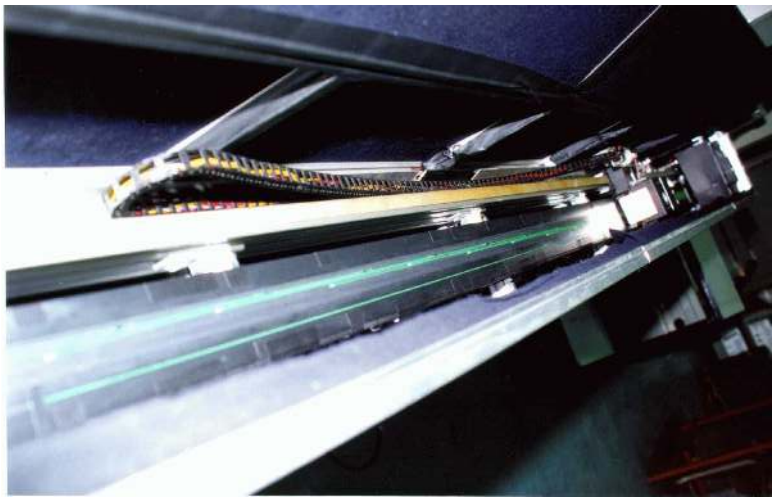

Figure 15: The pigtail scanner used to test the pigtails produced for all the HO trays

The pigtails are tested with the help of a setup specially built for this purpose (see Figure 15). The setup consists of a computer controlled mechanical stage which houses an UV lamp. The lamp is moved over the pigtail in controlled steps. At specific points, the shutter is opened, fibres absorb UV photons and the re-emitted light in each fibre is carried to the end to a set of photo diodes. Signals from the photo diodes are then digitised and stored in a data file. The combined transmission loss due to the spliced junctions, connector interface and attenuation offered are estimated by analysing these data.

The pigtail is connected through an optical connector to a set of 16 WLS fibres permanently mounted on the setup. The clear fibres of the pigtail are closer to this optical connector. Light from the UV lamp gets absorbed only when

the lamp is above a WLS fibre (not on a clear fibre). Readings are taken with the lamp at various positions on both sides of the optical connector. The difference between the two sets takes care of some systematics due to reflection at the connector. Measurements are made for all the pigtails belonging to a given layer and ring and if a pigtail is within 10% of the average in term of transmission properties, the pigtail is accepted.

Splicing quality of the fibres over the period of production is monitored by measuring the transmission efficiency between several composites of two WLS firers, before starting actual splice session on each day. The mean transmission efficiency and its spread over the entire production was found to be about 95% and 3% respectively.

4.2 Radioactive Wire-source

For the who;e barrel and endcap hadron calorimeter detector, the wire-source test [2, 6] is designed to be an in-situ relative tile calibration procedure. This was used as a quick quality control test of a completely assembled HO tray. Each of the assembled trays is tested for its response to open radioactive source. Each tray is equipped with a thin stainless tube which can route a wire carrying radioactive source on its tip across the tray. A stainless steel wire with a point-like radioactive source (Co^{60}) of approximate strength of 3 millicurie is wound as a coil and kept in a garage position inside a lead container (see Figure 16). This wire is pushed through the stainless steel tube attached to the tray by a remotely controlled system of drivers. The DC signal induced by the source traversing one tile of a tower provides an accurate measurement of the response of the entire measuring chain. Change of response due to photo-detector or electronics shows up as a change of the response of all tiles of a given tower and is compensated by an adjustment of the overall calibration factor.

Figure 16: The driver of the radioactive source tubes which is used to test the HO trays

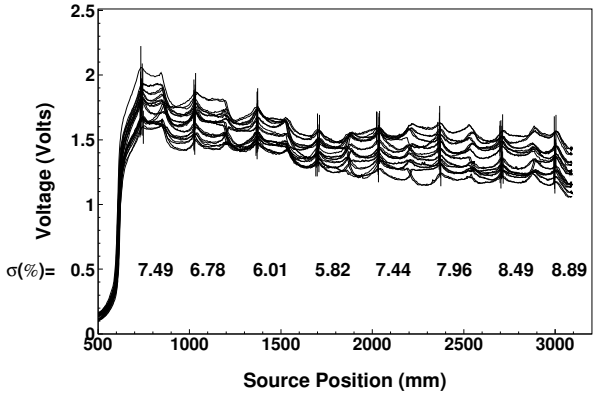

Figure 17: Wire Source scan of a set of 12 fully assembled scintillator trays (of the 12 sectors) belonging to ring 0 layer 0 tray position 3. The lines on the figures refer to the peak positions corresponding to the centre of the tiles and σ refers to the measured dispersions on those points.

The voltage output is monitored as a function of position of the Co^{60} source on the tray. It is monitored twice

during a run, once while stretching the wire and again while retreating to the garage position. Figure 17 shows the results from twelve such typical runs for the 12 trays belonging to ring 0 layer 0 tray position 3. The height of the signal is largest near the connector end (shortest fibre path) and there are several spikes which correspond to source positions where WLS fibre(s) directly see the effect of the source. The wire source response depends on the lateral size of the tile, the location of the source tube, and in a nonlinear way on the thickness of the scintillator. The dispersion in the response for each of these tiles is a measure of the quality of the tray. As one can see, the dispersion is well below 10% which is used as the acceptance criterion.

4.3 Radioactive XY Scan

Figure 18: The setup of the radioactive XY scanner which is used to test the HO trays

Each tray has also been tested with a radioactive source which not only scans along its length but also across its width. This scanner (see Figure 18) moves a collimated Cs^{137} (10 mCi) radioactive source housed in an appropriate lead container over the entire surface of a HO tray. The light yield is measured with the source placed at different points on the tray. The basic framework as well as the X-Y positioning mechanical sub-system of the scanner has been designed using extruded special aluminium channels. The stepper motor driven belt and pulley scheme has been used on X and Y drives. The positioning accuracy of the scanner is about 1 mm over a span of about 3000 mm $\times$ 500 mm. The X-Y motion control, its monitoring as well as light readout are implemented in terms of PC based control and driver hardware modules.

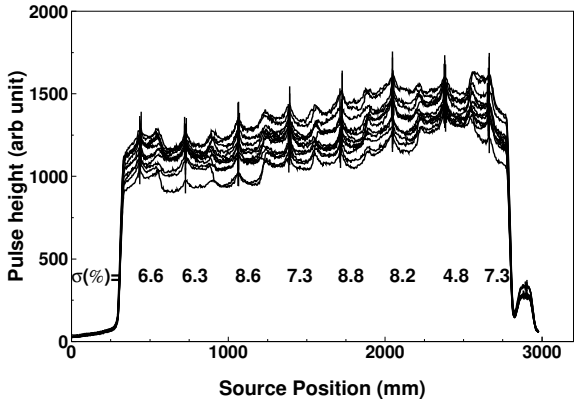

Figure 19: Scan of a set of 12 fully assembled scintillator trays (of the 12 sectors) belonging to ring 0 layer 0 tray position 3 using the XY scanner. The lines on the figures refer to the peak positions corresponding to the centre of the tiles.

Figure 19 shows the ADC output at several x and y points over the surfaces of twelve trays of tray type 3 belonging to ring 0 and layer 0. The collimated source excites all tiles in a similar way. One clearly sees that signal size for tiles close to the connector is largest and it slowly decreases for tiles with larger fibre length. The fluctuations

among the trays are at a level much below 10% which is used as the acceptance criterion for the trays.

A scintillator tile which is permanently fixed on one end of the scanning table is used to cancel out day to day gain variations in the readout system. The little peak at extreme right (near source position 290 mm) in Figure 19 is the signal from this tile which is used to normalise signals from the trays of the same group. The instrument is also used for obtaining the response uniformity scan of the entire tray.

4.4 Cosmic Muon Test

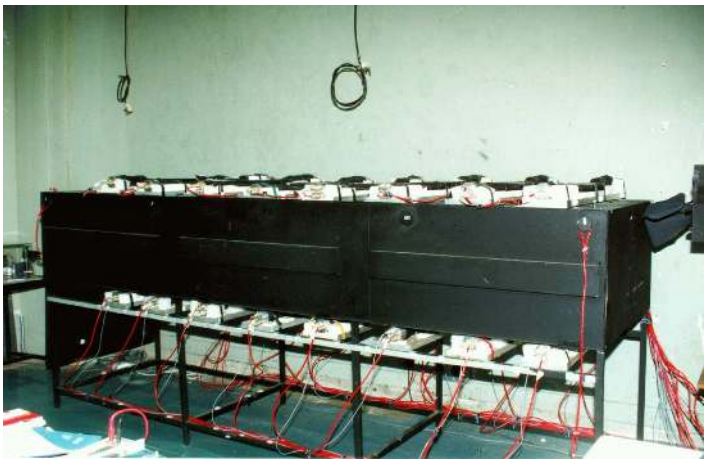

Figure 20: The setup for testing HO trays with cosmic muons.

The HO trays are expected to supply at least 10 photo electrons for a minimum ionising particle if a PMT were used in the read out. The completed trays have been tested for their responses to MIPs using cosmic rays in a special stand designed for this purpose (see Figure 20). The tray is placed in a black box equipped with a set of 8 telescopes. Each telescope has 4 scintillators with photo multiplier read out. Vertical muons are selected using 4-fold coincidence trigger logic. These telescopes are positioned roughly at the centre of each of the tiles in the tray. If any of the telescopes registers a coincidence, data from the tray are read out together with the information of the telescope causing the trigger (using a latch circuit).

Signal from the tiles are grouped into two bunches (alternate tiles) and the two bunches are then led to two fully calibrated green extended photo multiplier tube. The electronic signal is sent to a charge-sensitive ADC for converting it into a digital one. Online data are acquired in a PC via GPIB-CAMAC interface. These PMT's are calibrated using a precisely controlled LED source to get the factor for ADC count per photo electron.

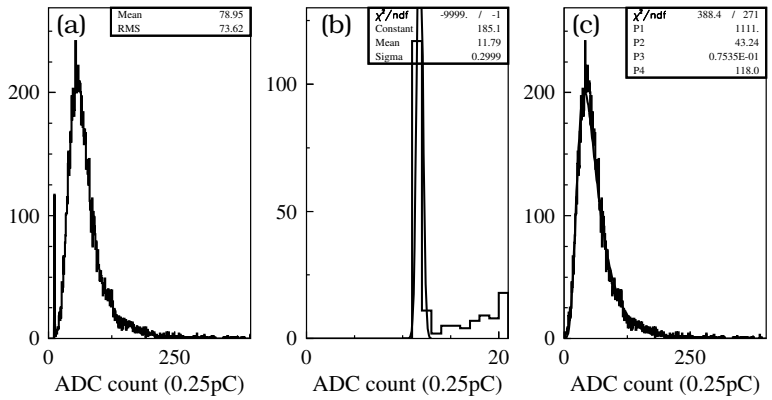

Figure 21: (a) Raw ADC spectrum for tile # 8 for one of the trays for ring 0 layer 0 tray position 3; (b) a fit to the pedestal part to a Gaussian distribution; (c) pedestal subtracted distribution fitted to a Gaussian convoluted Landau distribution.

Data are monitored online and there is a calibration tile equipped with fibre readout which is placed separately and

is always read out to monitor PMT gains. The pulse height spectrum is analysed offline to determine the number of primary photoelectrons produced. Figure 21a shows a typical ADC spectrum. One sees a very clear peak due to the passage of cosmic muons well separated from the pedestal peak. The position of the pedestal is obtained by fitting a Gaussian (see Figure 21b) to the pedestal part of the spectrum. The pedestal subtracted pulse height (see Figure 21c) is then fitted to a Landau distribution and the position of the mean value of the spectrum together with the calibration factor provides the number of photoelectrons yielded in a given tile.

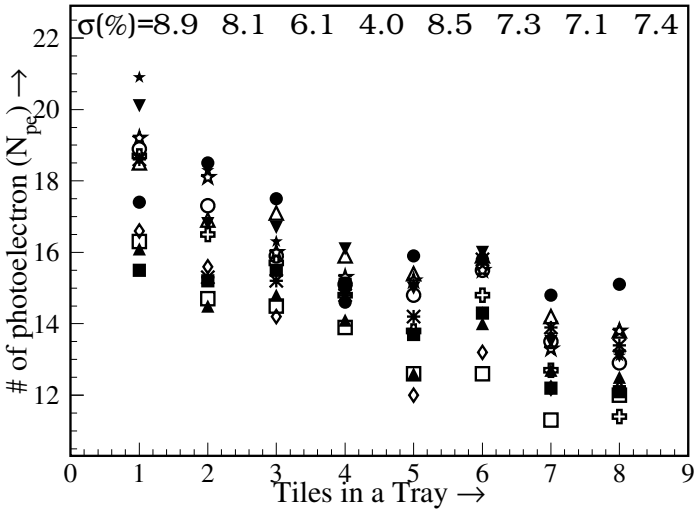

Figure 22: Number of photo electrons for the tiles in the set of 12 fully assembled scintillator trays (of the 12 sectors) belonging to ring 0 layer 0 tray position 3.

Figure 22 shows a plot of average number of photo electrons obtained using cosmic muons as a function of the tile number in a set of 12 trays belonging to ring 0 layer 0 tray position 3. The number of photo electrons is always above 10. They are as high as 20 for some of the tiles close to the connector. The RMS spread in the number of photo electrons is less than 10% which is the acceptance criterion for the trays.

4.5 Correlation of Calibration Constants

Correlation between all these three tests are shown in Figure 23. One finds that they are fully correlated. The same set of readout system is used for cosmic and wire source test, whereas a different PMT, optical connectors are used in the XY-scanner. Statistical error on these measured variables are less than 1%.

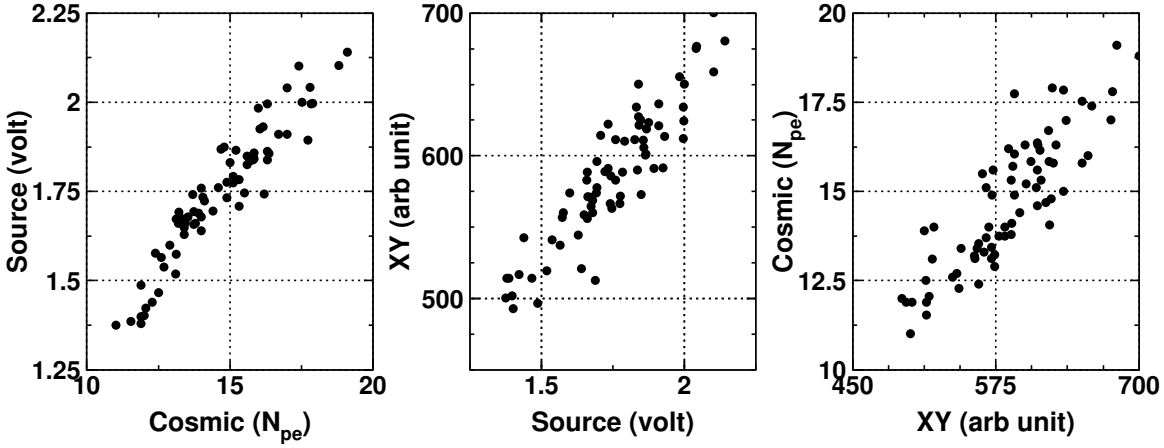

Figure 23: Correlations between number of photo-electron in cosmic test and signal peaks in the wire source and XY source test.

4.6 Tests at CERN

All the trays were again tested with radio active sources (both with wire source as well as with XY scanner) once the trays were received at CERN. All trays were found to be good at CERN. The two sets of measurement are seen to be fully correlated as can be seen in the Figure 24.

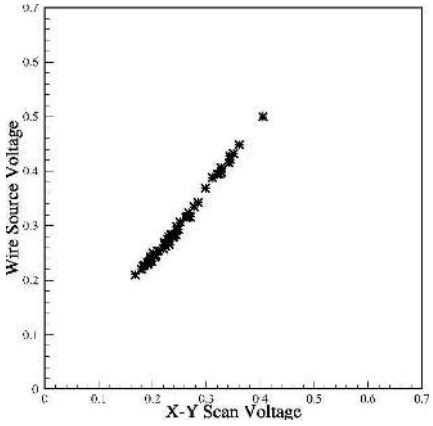

Figure 24: Correlation of the signal peak positions in the wire source and XY scans on the same tile as measured at CERN.

5 Hanging Structure

There is a maximum of 40 mm of clearance for placing the HO trays together with the hanging structures. Each tray with all its packing is expected to have a thickness of 15.44 mm. This necessitated a space of $17.0^{+0.2}_{-0.0}$ mm for inserting the trays. The total weight of a ϕ sector (six trays) is expected to be 30.0 kg. To support this weight, a possible design was to have a pair of aluminium honeycomb panels clamped between three C-channels on the two sides and one end keeping the other end open for inserting the trays. Engineering drawing of one such panel is shown in Figure 25.

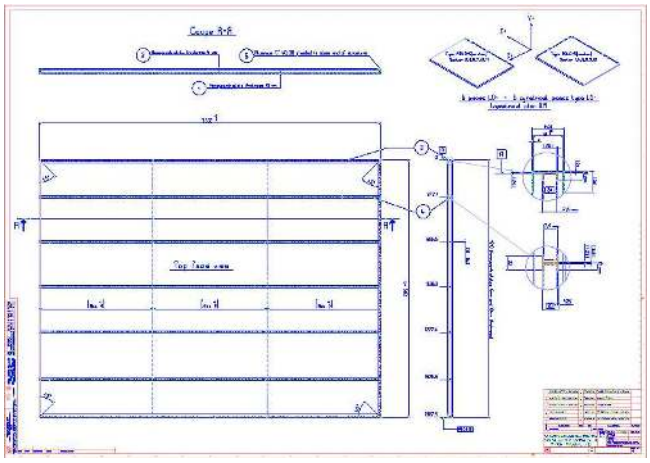

Figure 25: Engineering drawing of the support structure for ring 0 layer 0.

The hanging structure is made of aluminium honeycomb panels of thickness 10 mm for the bottom and 6 mm for the top. The top and bottom panels are put together with 20 mm $\times$ 40 mm aluminium C-channels glued by araldite on the 3 sides from outside and a set of twelve 20 mm $\times$ 20 mm aluminium C-channels glued on the inner side at a fixed separation for inserting the trays. The separation is properly adjusted for the appropriate tray width. Three sets of widths for a set of 72 panels are given in Table 4. The length of all the panels is kept at 2530^{+5}_{-0} mm. The widths of the three types of panels are respectively 1920^{+2}_{-0} mm, 2050^{+2}_{-0} mm and 2190^{+2}_{-0} mm. Panels for rings ± 1 and ± 2 also carry cooling tubes on one side. These serve as thermal screens to prevent heat percolation to the RPC/muon chamber assembly. The cooling tubes are made of copper and have inner and outer diameter of 6 mm

and 8 mm. These are glued to the 6 mm thick honeycomb surface using araldite and fixed with copper collars. For rings ± 1, a special panel is built to accommodate the short trays due to the chimneys.

Figure 26: A fully assembled panel of HO being mounted on one of the outer rings (ring $+2$) of the magnet yoke.

Ring	Layer	Width along ϕ in mm					
		Tray 1	Tray 2	Tray 3	Tray 4	Tray 5	Tray 6
0	0	278.9	347.1	336.5	331.4	331.4	272.6
0	1	304.3	367.9	356.6	351.2	351.2	296.8
$\pm 1, \pm 2$	1	321.9	370.1	358.8	353.3	353.3	410.7

Table 4: Widths of the slots in the hanging structure panels for the HO trays.

Glued joints of many of the honeycomb structures made for mounting the scintillator trays failed on application of very little force. All panels were subsequently repaired by screwing all the inner C-channels to the honeycomb structure using countersunk screws specially made for this purpose. These panels have been tested for withstanding a much higher pressure than they are expected to hold. Figure 26 shows one of the panels, fully loaded with HO trays, being lifted to be fixed in its location on the magnet yoke.

6 Test Beam Studies

Prototypes of HO trays were put together with 2 wedges of HB and a prototype of one sector of endcap hadron calorimeter module (HE) in the test beam facility at CERN. These prototype trays were exposed to a variety of positively as well as negatively charged beams of hadrons, electrons and muons over a wide energy range. These tests have been carried out over a number of years. Figure 27 shows a picture of the test beam area with the layers of HO trays as in the 2002 setup.

6.1 Synchronisation Study

Arrival time of signals from a scintillator tile to the readout element has a significant dependence on its location in η. Energy is measured by summing over a number of time slices and this η dependent time of arrival makes the energy measurement rather complex. This effect has been taken care of by introducing an appropriate η dependent delay for each of the towers. These delays have been obtained from a study of the test beam (2004) data with muons and pions (see Figure 28).

6.2 Calibration

During the 2004 test beam experiment HO trays were calibrated using the radioactive wire-source test (as described in Section 4.2) as well as by exposing them to a to a beam of monochromatic muons. While analysing the wire source data, the reel position is used to find out the correspondence between tile number and readout channel. Figure 29 shows a plot of ADC counts from ring 0, layer 0 tiles as the radioactive source passes along them. Pedestal is determined by fitting a straight line with zero slope to the part of the signal when radioactive source is far away from the tile under consideration. Peak value of the signal from a tile after pedestal subtraction is taken

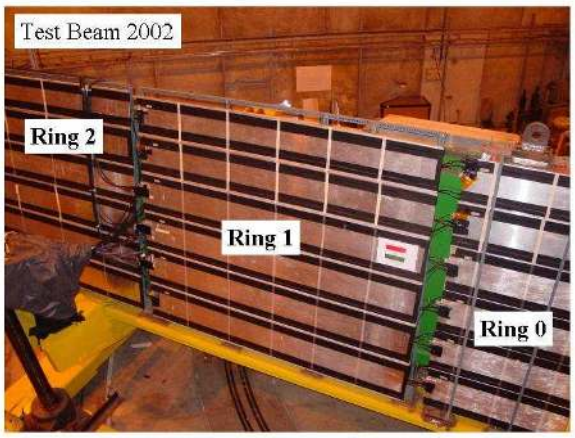

Figure 27: Picture of the test beam area during the 2002 setup. The HO trays are marked in the picture.

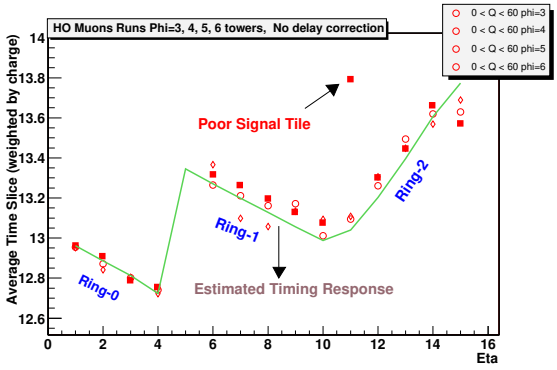

Figure 28: Charge weighted average time slice as a function of η index of the tiles in HO before the time delay correction.

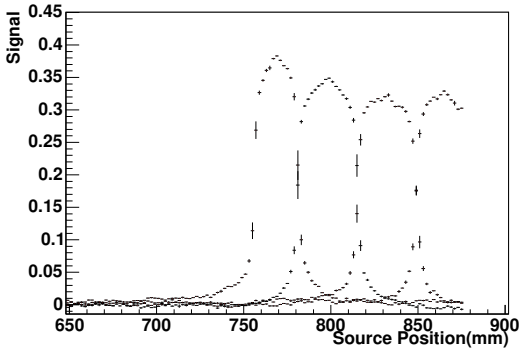

Figure 29: ADC counts from ring 0, layer 0 tiles as the radioactive source passes along them.

as the calibration constant for that tile. The HPD for HO readout was operated at voltages 8 kV and 10 kV and separate datasets were collected for the two settings. Calibration constants obtained with these two sets of data show the expected consistency (see Figure 30) being different by a factor of 1.415.

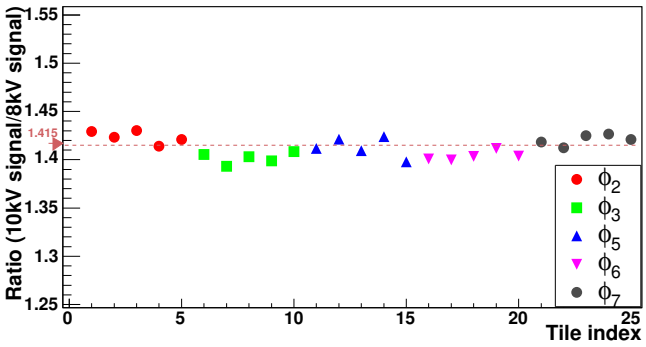

Figure 30: Ratio of calibration constant for ring 1 HO tiles in the test beam set up with the HPD's being operated at 10 kV and at 8 kV.

For the muon runs, the HPD was operating at 10 kV. Muons of energy 150 GeV were pointed at the centre of each HO tile and the ADC signal from the tile was used to find the muon calibration constant. To minimise noise, the sum of 4 time slices with the maximum amount of energy deposit is taken as the signal. The sum of four time slices away from the signal region is taken as the pedestal. The pedestal and signal peaks are not well separated in all the tiles (particularly in ring 1). The pedestal value is taken as the fitted mean obtained by fitting the pedestal distribution with a Gaussian curve. The peak region of the pedestal subtracted muon signal is then fitted with a Gaussian convoluted Landau distribution and the mean from this distribution is taken as the muon calibration constant for the tile. Figure 31 shows correlation plot of calibration constants obtained through the two sets of measurements.

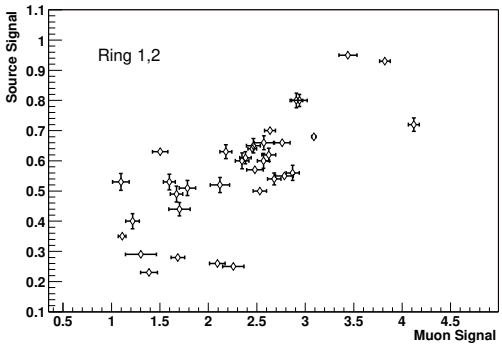

Figure 31: Calibration constant from muon signal plotted against the corresponding value from the wire source analysis.

6.3 Energy Measurements

Figure 32 shows energy distributions for a 300 GeV pion beam (from the 2002 test beam studies) with only HB in the beam and with HB+HO in the beam. The measured distributions for hadron beams of energy above 100 GeV are more symmetric and have smaller widths after adding HO to the energy calculation. This confirms the expectations from simulation studies shown in Section 2.

6.4 Muon Trigger

The signal size due to penetrating beam is compared with the noise level in the HO tiles from the 2002 test beam studies (see Figure 33). This study has indicated that HO will be able to provide signals for minimum ionising particles with efficiency better than 90% keeping the noise level below 20%. CMS uses signal in the Resistive

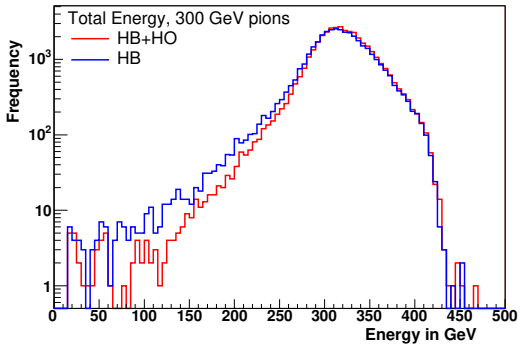

Figure 32: Energy distribution for a 300 GeV pion beam with only HB and with HB + HO in the beam.

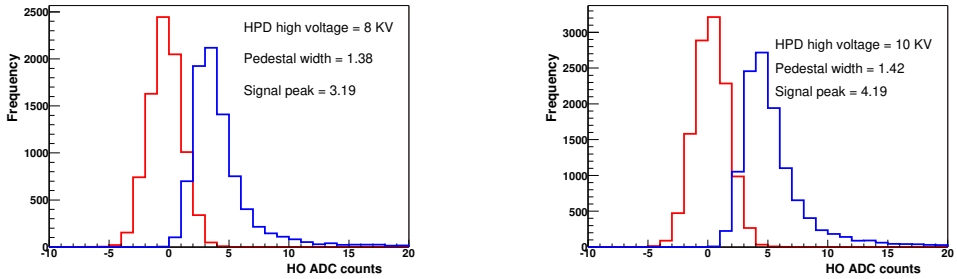

Figure 33: Pedestal peak and muon signal for a ring 2 tile operated with a voltage of (a) 8 kV, (b) 10 kV on the HO HPD.

Plate Chambers (RPC) to trigger for muons in the barrel as well as in the endcap region. In the barrel (RPC trigger towers 1-6) and in the overlap region (RPC trigger towers 7-9) for the RPC's, there is a considerable coverage by HO. Even with 95% chamber efficiency of the RPC's, muon trigger efficiency is rather poor for RPC trigger towers 6-9 (as low as 72%) if only RPC's are used in coincidence. This study suggested that HO could be a useful component in muon trigger together with the RPC at these solid angle[7].

As it has been observed for data collected with the radioactive source, size of the signal collected from HO tiles is considerably bigger when the HPD is operated at 10 kV as compared to 8 kV. This is also demonstrated in the HO signals obtained from the 2002 test beam studies with 225 GeV/c muon beam, as shown in Figure 33. In view of these data, the HPD's for HO will be operated at 10 kV in the CMS experiment. Use of HO will make the trigger efficiency better than 90% over most of the solid angle. Figure 34 shows a plot of efficiency of muon detection versus purity of the signal obtained from the 2003 test beam studies.

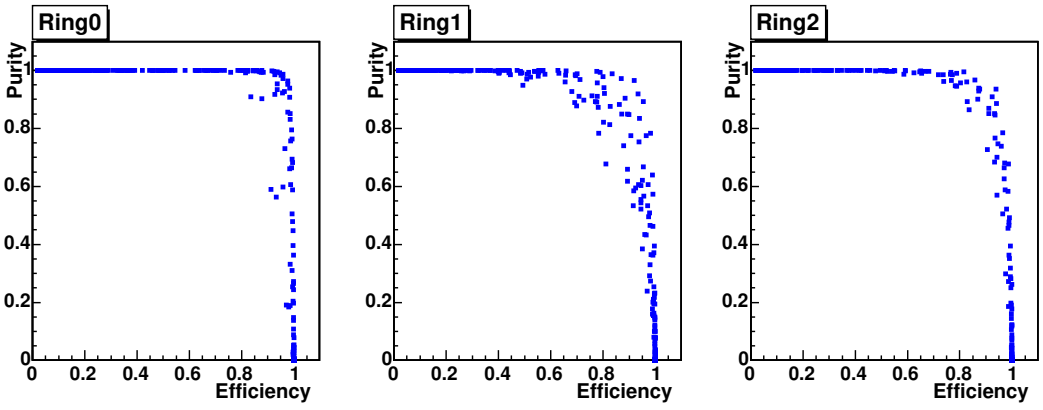

Figure 34: Efficiency vs. purity of muon detection in HO detector.

7 Summary

Constrained to lie outside of the inner CMS detector layers (pixels, tracker and electromagnetic calorimeter) and inside the 4 Tesla magnet, the hadron barrel calorimeter was found to be too thin to effectively absorb high energy hadrons specially near the η = 0 region. This would lead to degraded sensitivity for establishing new physics signals whose main signature is missing $\mathrm{E_T}$. The addition of sensitive detector layers just outside the magnet (inside the first barrel muon station) was simulated and shown to ensure much smaller energy leakage and hence improvement in the energy resolution.

Sensitive detector layers of 1 cm thick plastic scintillator with embedded WLS fibre readout (similar technology as the CMS barrel and endcap hadron calorimeters) were selected as the appropriate detectors. The responsibility of fabrication and installation of this outer hadron calorimeter (HO) was given to the Indian groups from Panjab University and Tata Institute.

References

[1] CMS Technical Proposal, CERN/LHCC 94-38, LHCC/P1, December 15, 1994.

[2] CMS Hadron Calorimeter Technical Design Report, CERN/LHCC 97-31, CMS TDR 2, June 20, 1997.

[3] CMS-HCAL Collaboration – V. V. Abramov *et al.*, Nuclear Instruments and Methods **A457** (2001) 75.

[4] Sudeshna Banerjee and Sunanda Banerjee, CMS Note 1999/063.

[5] Outer Hadron Calorimeter Engineering Design Review, TIFR/CMS-99-01.

[6] E. Hazen *et al.*, Nuclear Instruments and Methods **A511** (2003) 311.

[7] C. Albajar *et al.*, CMS Note 2003/009.